International Journal of Applied Earth Observation and Geoinformation 134 (2024) 104201

Contents lists available at ScienceDirect

International Journal of Applied Earth Observation and Geoinformation

journal homepage: www.elsevier.com/locate/jag

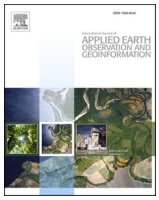

UAV and field hyperspectral imaging for *Sphagnum* discrimination and vegetation modelling in Finnish aapa mires

Franziska Wolff [a,*], Sandra Lorenz [b], Pasi Korpelainen [a], Anette Eltner [c], Timo Kumpula [a]

[a] Department of Geographical and Historical Studies, University of Eastern Finland, Yliopistokatu 2, P.O. Box 111, Joensuu 80101, Finland
[b] Division Exploration Technology, Helmholtz-Zentrum Dresden-Rossendorf, Helmholtz-Institute Freiberg for Resource Technology (HZDR-HIF), Chemnitzer Straße 40, Freiberg 09599, Germany
[c] Institute of Photogrammetry and Remote Sensing, TUD Dresden University of Technology, Dresden 01062, Germany

ARTICLE INFO

Keywords:
Peatland
Hydrology
Spectral library
Water index
Classification
Spectral Angle Mapper

ABSTRACT

Detailed knowledge of vegetation patterns allows to evaluate mire ecosystems and their dynamics. The use of hyperspectral information has the benefits of exploring spectral characteristics of species and vegetation modelling. Our study employed multi-scale and multi-source hyperspectral imaging with a handheld camera in the field and an UAV (Unoccupied Aerial Vehicle) sensor covering the wavelengths of 400 – 1000 nm. Plot-level spectra acquired with a UAV and field spectra collected at 1 m height were combined to develop a spectral library for *Sphagnum* moss species. This library was then used to map dominant *Sphagnum* species in a Finnish Aapa mire complex using the Spectral Angle Mapper (SAM) classifier. Classification performance assessment was supported by calculating a water index from the UAV-information. Additionally, we examined the transferability of site-specific spectral libraries to an aapa mire with similar vegetation. The results showed little spectral variation in the plot spectrum between the sensors. A fusion of species- and plot-level libraries yielded the highest accuracy of 62 %. For both mires, there was a great variation among the class accuracies. Floating mosses had an accuracy of 86 %, followed by lawn-forming *Sphagnum balticum* with 77 %. For the test site, the latter species was mapped with an accuracy of 59 %. Red moss species achieved low accuracies of 45 % and 38 %, likely due to effects from sub-pixel and mixed-pixel effects of neighbouring graminoid species and the presence of litter. This might have also enhanced the contrast of adjacent pixels contributing to spectral alterations. Water table depth measurements and the water index revealed a hydrological preference for most species, with classification performance notably improving with higher water index values. We recommend collecting on-site hyperspectral information at varying hydrological circumstances to build a comprehensive spectral library for mire vegetation and modelling.

1. Introduction

Detailed vegetation modelling of peatlands is needed to support climate modelling, land use management, and restoration efforts in the face of environmental changes. In waterlogged peatlands, often referred to as mires, plant communities and species give insight into ecosystem functioning (Hájek et al., 2011; Korrensalo et al., 2016; Mathijssen et al., 2019; Ward et al., 2015). Here, *Sphagnum* mosses are good indicators for peatland dynamics and succession trends (Granath et al, 2010; Kolari et al., 2021), as they have certain water table depth and pH optima (Andrus et al., 1983; Andrus, 1986) and can be divided into generalist and specialist (Johnson et al. 2015; Tahvanainen and Tolonen, 2004). Changes in environmental conditions may result, however, in altered key species' spatial distribution and a shift from one successional stage to another (Laine et al., 2011; Väliranta et al., 2017). For instance, an increase of bog over fen vegetation has been observed for boreal peatlands (Granlund et al. 2022; Kolari et al. 2022) emphasising the need to monitor peatland dynamics and to recognize species distribution patterns, ideally under consideration of the hydrological site conditions.

Hyperspectral imaging is a part of remote sensing-based spectroscopy and gives the opportunity to assess these complex vegetation patterns and their link to hydrological site conditions. The added value is due to the narrow-band assemblage providing finer spectral details than by broad-band multispectral and RGB sensors. Important pigments are

* Corresponding author.
E-mail address: franziska.wolff@uef.fi (F. Wolff).

https://doi.org/10.1016/j.jag.2024.104201
Received 12 April 2024; Received in revised form 7 August 2024; Accepted 1 October 2024
Available online 11 October 2024

chlorophyll *a* and chlorophyll *b*, which strongly absorb visible wavelengths at approximately 430 and 660 nm, and at 450 and 640 nm, respectively (Chen and Blankenship, 2011; Lichtenthaler and Buschmann, 2001; Ustin et al., 2009). In contrast, carotenoids and sphagnorubin are responsible for the reddish coloration of some *Sphagnum* species. Carotenoids contribute to photosynthetic activities by absorbing light primarily between 400 – 500 nm and provide hues ranging from yellow to red (Harris, 2008). Sphagnorubin, on the other hand, causes absorption peaks around 500 – 550 nm leading to the intense red coloration observed in certain species (Berland and Andersen, 2021). Water content and water retention are also important, as water causes prominent absorption features at about 970 and 1200 nm (Caturegli et al., 2020; Clevers et al., 2008; Granlund et al., 2018).

The required spectral information can be recorded with different sensors and platforms. Common point spectrometers used in proximal sensing excel at capturing spectral features of species in the laboratory or plant communities in the field but lack spatial information. In contrast, satellite images and data collected from Unoccupied Aerial Vehicles (UAVs) provide spatially explicit information over larger areas. Spectral imaging devices for field data collection offer an intermediate solution by combining spectral and spatial information at species level. Acquiring field-collected species data, in addition to UAV data, helps in understanding spectral responses at different spatial scales (Rautiainen et al., 2018). Field spectra can provide a fine level of detail needed to upscale information, as challenges arise when directly coupling laboratory with satellite- and UAV-based remote sensing products (Bubier et al., 1997; Cole et al., 2014a; Erudel et al., 2017; Harris et al., 2015). However, variations in acquisition altitude and remote sensing platforms cause differences in the retrieved spectra. Common reasons include mixed pixels, atmospheric noise, and the adjacency effect (Kaufman, 1984), which involves the influence of neighboring pixels on target pixels, altering their spectral characteristics. Spectral information of different platforms or sensors can be stored as spectral libraries across different wavelengths. Accessible mire vegetation data in form of spectral libraries has been scarce (Salko et al., 2023). The risk of using available plant spectra information is the temporal mismatch between the library reference data and the image data used for the modelling process. Nevertheless, the selection of spectral libraries expands gradually (Kokaly et al., 2017) and is used for vegetation analysis (Cunnick et al., 2023).

Previous vegetation modelling or classification has usually been constrained to peat- and wetland types, plant functional types (PFTs), and plant communities (Cristóbal et al., 2021; Schaepman-Strub et al., 2009; Schmidt and Skidmore, 2003). The accuracies vary between moderate and good, often declining with increased vegetation detail or higher heterogeneity, favouring four to five classes linked to distinct micropatterns (Arkimaa et al., 2005; Middleton et al., 2012; Räsänen et al., 2020). However, feedback mechanisms, triggered for instance by variation in photosynthesis rate and species composition (Breeuwer et al. 2008; Kokkonen et al., 2022; Robroek et al., 2007), require species level information. Here, UAVs are advantageous, as they provide a high spatial resolution relevant to monitor complex vegetation patterns such as in mires, and in turn cover a larger spatial extent with more side-variation than field imager or spectrometer. The development of hyperspectral UAV sensors allows capturing site conditions at a spectral and spatial scale that is relevant for mire vegetation modelling. The substantial interplay between vegetation type, hydrological conditions, and spectral response, specifically due to the water retention capabilities of *Sphagnum* mosses (Bryant and Baird, 2003; Meingast et al., 2014; Neta et al., 2011; Stuart et al., 2022) likely can be recognized using UAV-based spectroscopy. Hydrological variables, such as water content and prevailing moisture, affect the spectral responses of species (Arkimaa et al., 2009, Harris et al., 2005), posing a challenge for image classification. Despite this indispensable relationship, research has been limited to laboratory assessments in controlled environments. For large-scale remote sensing-based assessments, it is essential to understand the in-situ spectral information of moss species and how mapping accuracy varies along hydrological gradients, acknowledging that side conditions impact spectral properties and modelling performance. Our study therefore aims to contribute to peatland monitoring, allowing for a more comprehensive understanding of data acquisition times and shed light on potentially needed hydrological correction factors.

Showcasing two aapa mires in North Karelia, Finland, and using field hyperspectral handheld and UAV-information, this study 1.) explores the potential and limitations of multi-source and multi-scale spectral libraries to model the distribution of dominant *Sphagnum* mosses, and 2.) examines the spatially varying impact of hydrological conditions on classification.

2. Research sites and data acquisition

2.1. Research sites

The research sites situated in North Karelia, Finland, represent typical aapa mire complexes with fen and bog features and micropatterns (Fig. 1). They are characterized by elevated hummock formations and lower lawns at the margins typical for bogs, as well as wet areas referred to as (wet) flarks with occasional water at the surface crossed by hummock-forming strings as fen characteristics. The transition between bog and fen is marked by lawns and carpets of *Sphagnum* mosses.

An overview of the prevailing species can be found in Table 1. Ilajansuo mire served as the research site, for which all data sets have been acquired. Viitasuo mire was our test mire, at which we applied the developed approach. Although this aapa mire shows the same elements as Ilajansuo mire, we selected an extent that excluded the wet flark area to a large share (see Section 2.5).

2.2. Data collection

2.2.1. Vegetation collection

We collected vegetation data from field plots with species inventory from 32 locations in August 2022 focusing mainly on homogenous *Sphagnum* moss plots using a 30 x 30 cm^2 vegetation square (Table 1). The vegetation plots were selected randomly but as spatially equally as possible with plot locations chosen to be both representative and surrounded by minimal variation in the immediate neighbourhood. Additional plots with the same dimension from a previous field work session in 2020 served as a more comprehensive data set. This original dataset was collected over a larger area using a stratified random sampling approach aimed at modelling plant communities, as described in Wolff et al. (2023). Within the study extent of this research, 40 plots featured a mix of nearly pure *Sphagnum* mosses and mixed vegetation relevant to this study. The plot locations were measured with Trimble R10 RTK-GNSS (Real-Time Kinematic Positioning-Global Navigation Satellite Systems) providing coordinates with 1–2 cm accuracy. Species identity and coverage in percentage was noted. For Viitasuo mire, 24 vegetation plots documented using the same stratified random sampling scheme as for Ilajansuo mire during the same field campaign in 2020 were used in this study. For each plot at both sites (in Ilajansuo for both years), we noted down the water table depth (WTD).

2.2.2. Handheld imagery

Handheld hyperspectral imaging of the 32 vegetation plots was done on 11 August 2022 under clear sky conditions with occasional clouds using the push-broom camera Specim IQ by Specim Ltd covering a wavelengths range of 400–1000 nm with a resolution of 512 x 512 pixels and 112 spectral bands. Image acquisition was only carried out under clear sky conditions from approximately 10 AM until 6 PM. The device was placed on a tripod with approximately 1 m between camera and vegetation plot.

Wet locations of the flark were left out because the tripod did not

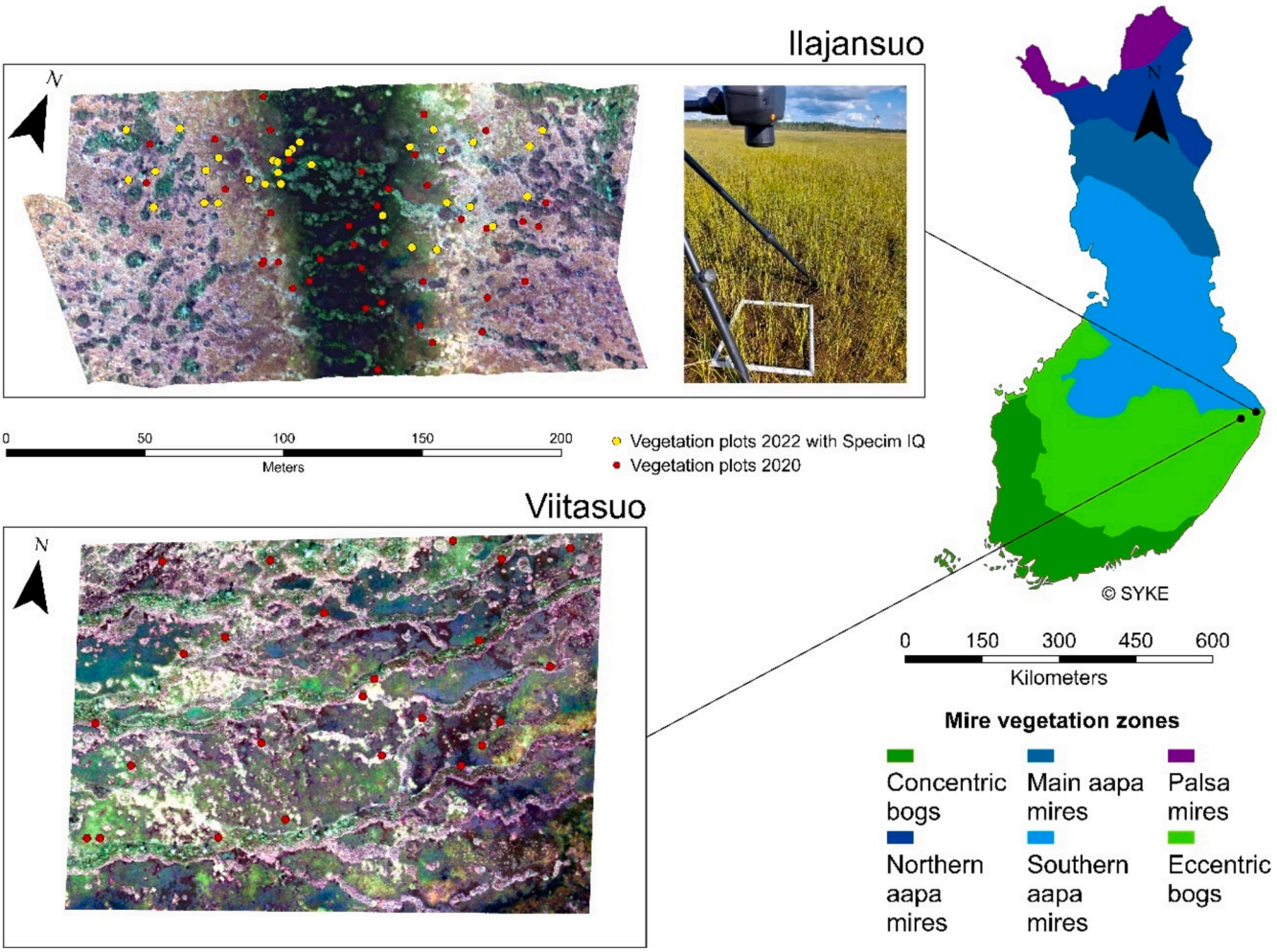

Fig. 1. The aapa mires Ilajansuo and Viitasuo and their location along the mire vegetation zones in Finland (© SYKE, Finland) shown using RGB-band combinations of the hyperspectral UAV data (R: 676 nm, G: 541 nm, B: 435 nm). Vegetation plots of 30 x 30 cm collected in the years 2020 and 2022 are shown in red and yellow markings, respectively. The latter indicated those plots, for which Specim IQ handheld hyperspectral images were recorded according to a setup shown in the image.

Table 1
Species present in the vegetation plots of Ilajansuo.

***Sphagnum* mosses**	**Graminoids**	**Other vascular plants**
Sph. balticum	*Eriophorum vaginatum*	*Andromeda polifolia*
Sph. fuscum	*Scheuchzeria palustris*	*Betula nana*
Sph. jensenii	*Carex limosa*	*Empetrum nigrum*
Sph. medium coll.	*Carex rostrata*	*Drosera anglica*
Sph. majus	*Carex chordorrhiza*	*Drosera rotundifolia*
Sph. papillosum		*Rubus chamaemorus*
Sph. rubellum		*Vaccinium oxycoccos*
Floating mosses		*Vaccinium vitis-idaea*

remain stable. Under field conditions with unsteady ground, we employed a spirit level to reach an angle as close to nadir as possible. For each of the 32 vegetation plots, handheld imagery covered the entire vegetation square and was acquired with two or three replicates for each plot to compensate for possible changes in illumination and change in sun angle. The exposure time varied depending on the lighting conditions. During the recordings, we placed a close to 100 % Spectralon® white reference panel next to the frame.

2.2.3. UAV-imagery

The UAV hyperspectral flight was carried out with the push-broom camera Specim AFX 10 by Specim Ltd at an altitude of about 100 m under clear sky conditions in Ilajansuo on 11 August 2022 and in Viitasuo on 8 August 2023 at approximately solar noon. This sensor covered the wavelength range from 400 – 1000 nm with spectral binning of 4 resulting in 112 bands of 5.5 nm spectral resolution for the imagery. Spectral binning compressed these to 112 bands. The UAV-data of Viitasuo mire acquired at the same point in time one year later allowed testing the temporal robustness of spectral libraries in a similar mire with known vegetation. For radiometric calibration and correction, three different calibration targets were spread with a reflectance of 2 %, 9 %, and 46 %. For Ilajansuo mire, we placed three Ground Control Points (GCPs) and recorded the position of these with RTK-GNSS device. In addition to the hyperspectral flight, we also conducted a multispectral UAV-flight with MicaSense Altum PT in both sites covering a slightly larger area. These were used in this study only for the enhancement of georeferencing facilitated by the built-in RTK positioning system.

3. Methodology

The workflow consists of processing the image data, the establishment of three different spectral libraries for image classification using the Spectral Angle Mapper (SAM), and the performance assessment. Key steps are here the spatial variation assessment of the target species and vegetation plots, as well as the accuracy assessment and water index (WI) explaining the SAM results. Fig. 2 provides an overview of these essential steps that are elaborated on in this section.

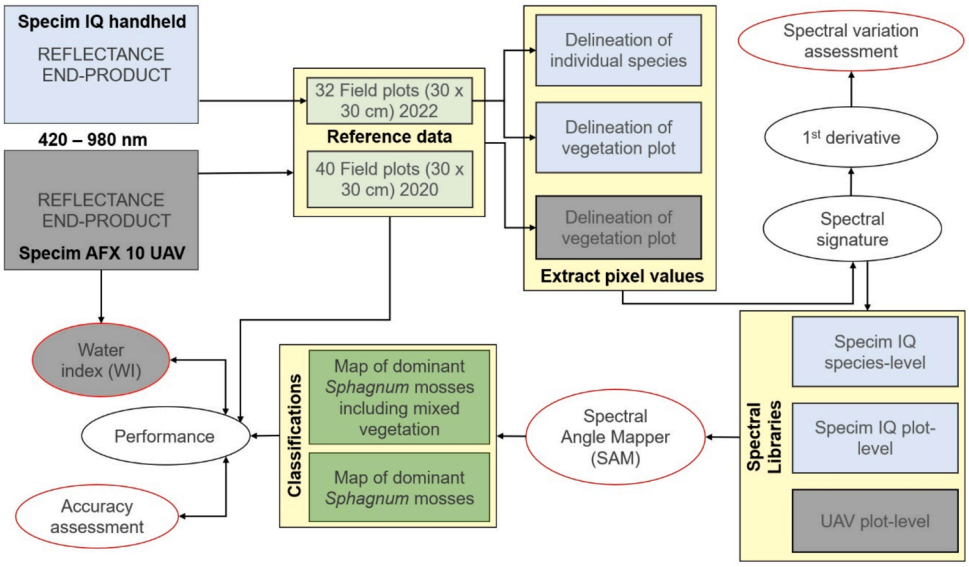

Fig. 2. The post-processing steps using the end-products of the hyperspectral image data. The grey shapes relate to the information derived from the UAV reflectance end-product and the light blue shapes the respective information from the handheld camera. Red outlined steps emphasise key aspects investigated in this study.

3.1. Data processing

The processing of the UAV-hyperspectral imagery with a spatial resolution of 8 cm involved several steps using the software ENVI version 5.6.3 (Exelis Visual Information Solutions, Boulder, Colorado) and CaliGeo Pro version 2.6.1, an ENVI plug-in created by Specim Ltd. First, the raw AFX 10 sensor data was converted into radiance data and georeferenced in CaliGeo Pro. The initial process involved subtracting the dark image from raw numbers, utilizing factory calibration data for spectral radiance conversion. The flight lines were georeferenced achieving centimetre-level horizontal accuracy by image alignment resulting in a high accuracy multispectral UAV orthomosaic. Reflectance values were obtained by incorporating reflectance panels visible in the UAV image. We applied an Empirical Line Correction in ENVI to correct for atmospheric influence. The image showed minimal noise throughout the entire image, with even illumination and very little shadow due to the flat terrain, thus, topographical corrections were not applied. Due to the flat terrain, no separate consideration of the sun angle was done. In opposite to the Specim AFX 10, the handheld device Specim IQ records for radiometric calibration a white and a dark reference image, of which the first refers to the calibration panel in the field. The dark reference is created automatically by closing the shutter of the camera during the recording. After the recording process, the device automatically retrieves the reflectance values with these. For further usage, we extracted the image pixels within the vegetation frame, while discarding the pixels from the frame itself, the adjacent shadow pixels, and those located outside of the frame. 2–3 image replica were available to account for possible changing circumstances. The spectral range of both devices was filtered to 420 – 980 nm with a total of 104 bands.

3.2. Spectral library preparation

Spectral information from the handheld and UAV images is stored in spectral libraries. Three separate libraries were created containing a) species level data from the handheld device, b) plot level data from the handheld device, and c) plot level data from the UAV sensor (Fig. 3).

At species level, the delineated regions of interest (ROIs) comprised at least 50 image pixels each, and for each species between 30–55 regions regardless of weakly or strongly illuminated pixel. The value of all pixels per species was averaged. The result was a spectral library with *Sphagnum* species labels for the classification process. For the second library all pixels within the vegetation plot recorded with the handheld device were extracted and averaged, representing plot level spectral information. The UAV plot-level library also used all averaged pixels within the vegetation plot (i.e., six image pixels). To each plot, labels of dominating *Sphagnum* moss species were assigned with the criteria that one moss species had to cover more than 80 % of the plot. This threshold to ensured the (spectral) dominance of the corresponding species.

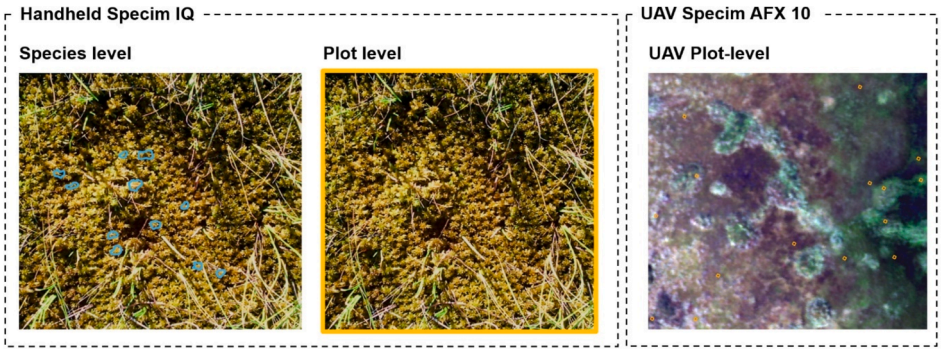

Fig. 3. Three spectral libraries stored the spectral information captured at different altitudes with the sensors Specim IQ and Specim AFX 10. Manually selected regions of interest (ROIs; blue outlines) delineated the pixels of the target species. At both plot levels, the pixels within the vegetation plot were used (orange frame and orange polygons).

Although the images revealed also other plants, we lacked sufficient spectral information of these to feed separate library entries. Due to mixed vegetation in the field, a separate entry labelled as such containing spectral information of *Andromeda polifolia*, *Empetrum nigrum*, *Eriophorum* spp., and *Rubus chamaemorus* in addition to spectrally abundant litter (i.e., dead biomass) was added. We labelled those plots as mixed vegetation, where the moss abundance was less than 80 %. It was not possible to record images in the wettest part of the mire that exhibits floating and submerged mosses. Therefore, the ROIs of the floating mosses were delineated on the UAV image and formed a separate library entry for the classifications.

3.3. Water index

We calculated a water index as a proxy for hydrological conditions in mires to investigate its impact on image classification. Based on the spectral profiles and available bands, we created the water index (WI) (Penuelas et al., 1997) using bands in the near-infrared region as follows:

$$WI = B_{900}/B_{950}$$

The relationship between the calculated Water Index (WI) and measured water table depths (WTD) in Ilajansuo mire for the year 2022 was assessed using statistical analysis in R (for more details, see section 3.5). Additionally, we had recorded WTD measurements for both mires in 2020. While recognizing the differences in measurements between the years, we assume that at species level the WTD changes may reveal a proportional relationship. Thus, we also compared the WI to the WTD of 2020 for Viitasuo mire while acknowledging that species may have different sensitivities to changes in water conditions.

3.4. Classification of UAV-data

We used the algorithm of Spectral Angle mapper (SAM) to classify the Ilajansuo mire with our multi-source and multi-scale spectral libraries. In addition, we applied these also to our test site Viitasuo mire that show the same aapa mire elements. An overview of the models and their spectral library input can be found in Table 2.

3.4.1. Spectral angle Mapper

Often used in hyperspectral image classification the SAM algorithm compares the spectral information of image spectra with reference (library) spectra and calculates the spectral angle for different combinations of bands. A smaller spectral angle indicates a better match between the spectral library as reference data and the image reference data. We employed the Python tool package Hylite (Thiele et al., 2021), where the angle threshold is automatically set to the smallest, most ideal angle for matching the spectra. Here, each pixel is classified by being assigned to the spectral library class that is the most similar. The inputs for the classification are the hyperspectral UAV image and the spectral libraries (i.e., either individually or as a combination). The output is a classification image and a rule image with the spectral angle information. SAM is a simple similarity measure for spectral mapping compared to machine and deep learning techniques. However, it reveals a low sensitivity towards illumination artefacts as it uses the spectral shape rather than the absolute magnitude (Kruse et al., 1993). The advantage of using SAM is that the "curse of dimensionality" does not apply to that method, while learning-based classifiers require a dimensionality reduction to minimize redundance in the data (Hughes, 1968).

Table 2
The Spectral Angle Mapper (SAM) models and the corresponding spectral library reference data divided into libraries using only mosses and those including additionally mixed vegetation. Listed is further the spectral origin of the libraries.

SAM	Spectral library: Moss	SAM	Spectral library: Moss + mixed vegetation
Model 1	Species	Model 5	Species
Model 2	Plot level	Model 6	Plot level
Model 3	UAV plot-level	Model 7	UAV plot-level
Model 4	Species + Plot level + UAV plot-level	Model 8	Species + Plot level + UAV plot-level

3.4.2. Accuracy assessment

Image classification accuracy is evaluated through a confusion matrix providing overall, user's and producer's accuracy. User's accuracy is the proportion of correctly classified pixels for a specific class, while producer's accuracy measures the proportion of correctly identified pixels out of the total actual instances of a class. The spectral libraries contained on purpose classes for which it was known that they do not or only to a small extent exist in the test site's UAV-image scene. If the algorithm does not correctly classify pixels into those classes, the success cannot be expressed as any statistical metric due to the inevitably missing reference data of these "missing" species. Thus, we will discuss the outcome in the entire context of classification accuracy rather than placing weight solely on a confusion metric.

3.5. Statistical analysis

The statistical analysis explored the influence of hydrology on species distribution, spectral angle selection, and the subsequent impact on classification performance. Due to the not normal distributed nature of our data, we chose exclusively non-parametric tests. We first applied the Spearman correlation between the numerical variables (i.e., WI, spectral angle) among the species classes to test whether there is a preference for these along a certain WI and spectral angle range. Thereafter, the Mann-Whitney/Wilcoxon rank-sum test compared for each species the classification outcome (correct and incorrect) against the WI and spectral angle to evaluate whether the classification performance is better or worse at a certain range of these variables. Post hoc tests included the Dunn's test for multiple comparisons after the Kruskal-Wallis test. To model the probability of correctly classified species as a function of angle and WI (i.e., combined impact), we employed a Logistic Regression Model. The water-saturated floating moss regions with occasional surface water were excluded from the statistical analysis. The analyses were performed with R statistical computing environment version 4.2.3 (R Core Team, 2022) using base R package for specific analyses and ggplot2 package for visualizations. The data were analysed for statistical significance with a confidence level (p-value) of 0.05 for all tests.

4. Results

4.1. Spectral variation across species and libraries

All species had similar complex and partly overlapping spectra, with some minor, small-scale variations below 0.05 in reflectance. These values represented averages derived from multiple measurements, and as such, some degree of natural variation is expected in real-world conditions. Spectral separation was evident in the visible range of the spectrum between 550 – 680 nm with the shift of the reflectance peak for the red mosses *Sphagnum medium* coll. and *Sphagnum rubellum*, as seen in the derivatives as features at 620 nm (Fig. 4). In contrast, *Sphagnum balticum* and *Sphagnum majus* exhibited a yellowish appearance between 500 – 600 nm, where carotenoids absorb light, highlighted as reflectance features in the derivative profile at 550 nm. *Sphagnum papillosum* showed a reflectance feature at 510 nm and absorption features at 640 and 660 nm. The red-edge range, characterized by a sharp increase in reflectance, is notably marked by a derivative peak around 710 nm. Generally, the visible range of the spectra exhibited clear differences as emphasized by the derivatives, while the near-infrared wavelengths indicated random variation.

There was only minor variation between the plot level signatures

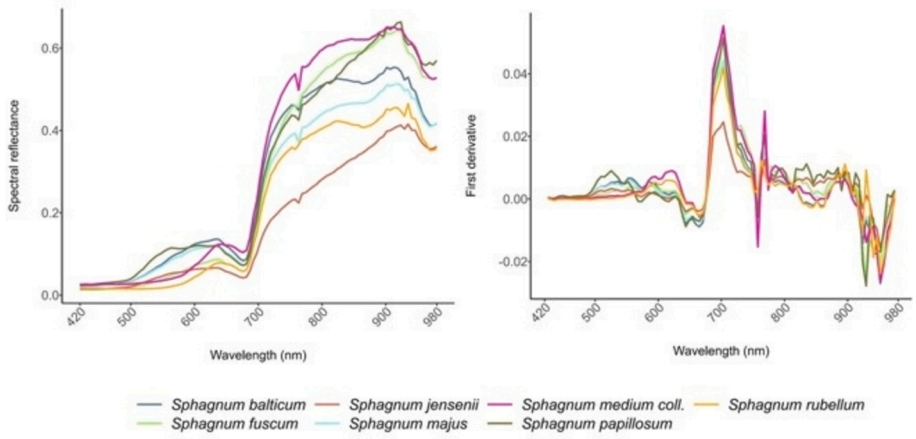

Fig. 4. Spectral profiles (left panel) and first derivatives (right panel) of *Sphagnum* mosses recorded with the hyperspectral handheld camera Specim IQ.

recorded from the two different sensors and altitudes despite the significant acquisition difference of 90 m (Fig. 5). The largest variation started at the red-edge region around 710 nm with about 0.05 in reflectance. The data used to set up the spectral libraries as recorded from different sensors and altitudes deviated predominantly in this specified region but stayed below 0.1. The first derivatives of Specim AFX 10 revealed at UAV-level random variation independently of the wavelength. Considering the individual species in this plot, *Andromeda polifolia* and *Rubus chamaemorus* had a reflectance peak at 550 nm, whereas *Sphagnum fuscum* reflected the strongest at approximately 650 nm. At this wavelength, also the plot level reflectance captured with both Specim IQ and Specim AFX 10 showed a reflectance feature. The reflectance properties at plot level (handheld and UAV) clearly showed a synergy of the three species' spectral contribution.

The most significant spectral variation was found in moss-dominated plots that host a variety of other vegetation types (i.e., *Sphagnum papillosum*-dominated). Despite these non-moss species covering only a small percentage of the plot, their contribution to the overall spectral mix was undeniable. This small share of spectral variation was distinct and significantly different from that of the mosses, resulting in a noteworthy cumulative effect, particularly on the overall spectral characteristics as emphasized by the UAV plot information (Fig. 6). Notably, the interquartile range remained within the range of 0.05 in reflectance up to 680 nm, after which it expanded to 0.12 in reflectance. *Sphagnum papillosum* is commonly found in flark strings, which include species such as *Betula nana*, *Andromeda polifolia*, *Drosera rotundifolia.*, and graminoids. As a result, this moss class expressed the highest level of diversity and hence, highest spectral variation.

4.2. Spectral angle Mapper

In our step-wise inclusion of the multi-scale and multi-source spectral libraries, we achieved good to moderate results for the classifications. The highest overall accuracy was 62 % for Ilajansuo mire including all libraries (Model 4; see Table 3). As a general trend, the models with the mixed vegetation reached lower accuracies for both mires.

Fig. 7 shows the location of the mixed vegetation, which was largely classified where either *Sphagnum fuscum*, the red mosses, or *Sphagnum papillosum* were present. These classes are expected to have the largest shares of miscellaneous vegetation, including litter.

Among the species, there was a noticeable misclassification trend between *Sphagnum jensenii*, *Sphagnum majus*, *Sphagnum papillosum*, and *Sphagnum balticum*. Although the class floating mosses achieved the best overall accuracy with 86 %, Table 4 points out that a share was misclassified as *Sphagnum jensenii*, which is a species of wet habitats that, among others, forms part of the largely submerged floating moss class.

At Ilajansuo mire, it became evident that the red moss species *Sphagnum medium* coll. and *Sphagnum rubellum* had the least accuracies (Table 4). While 28 % *of Sphagnum medium* coll. were detected correctly, the model incorrectly identified the remaining cases as *Sphagnum rubellum*, *Sphagnum balticum*, and *Sphagnum papillosum*. Conversely, the high user's accuracy of 63 % had the remaining instances being wrongly predicted as *Sphagnum rubellum*. The accuracies of this moss were opposite to those of *Sphagnum medium* coll. The producer's accuracy was moderate at 47 % (mainly misidentifying instances as *Sphagnum medium* coll.), while the user's accuracy was only 28 % due to misclassification

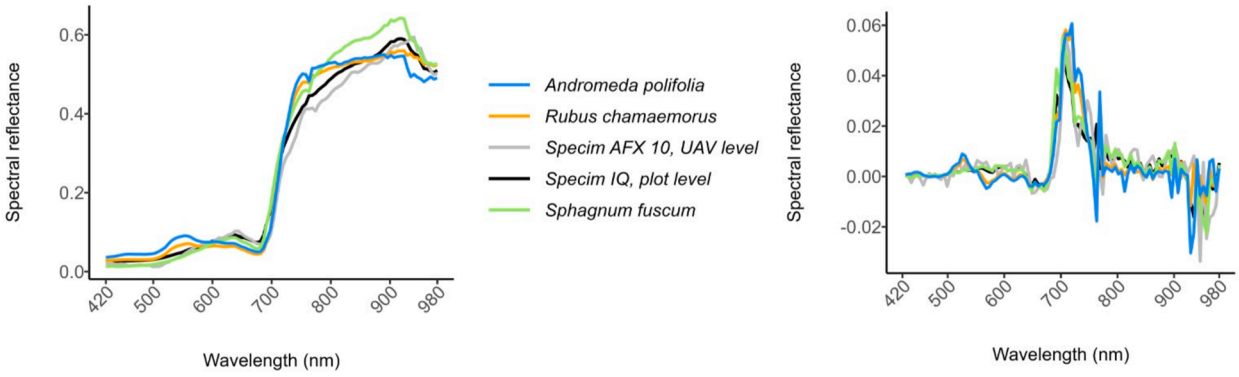

Fig. 5. The spectral deviation of a *Sphagnum fuscum*-dominated plot recorded at species- and both plot levels with Specim IQ (black line) and the UAV-sensor Specim AFX 10 (grey line). Species occurring in this plot are *Andromeda polifolia* (blue line), *Rubus chamaemorus* (orange line), and *Sphagnum fuscum* (green line). Spectral reflectance is displayed in the left panel and the corresponding first derivatives in right panel.

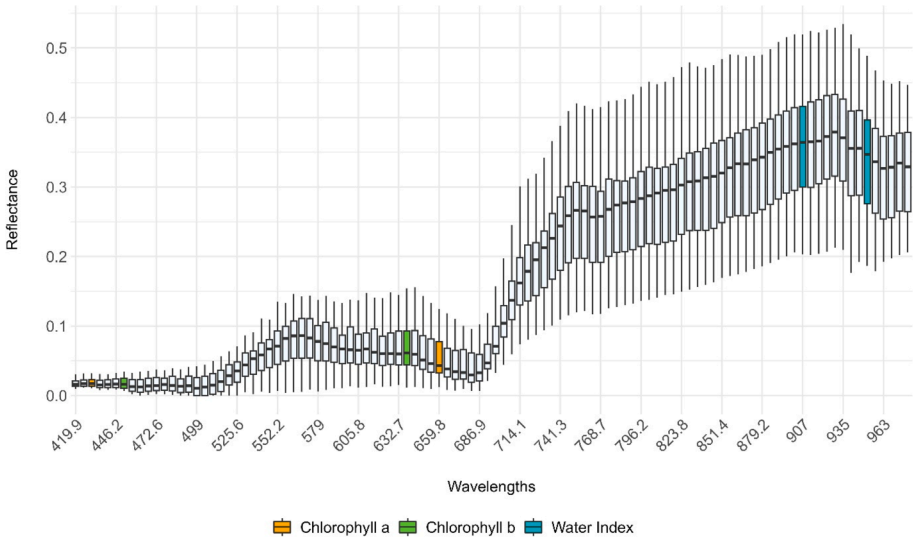

Fig. 6. Class-internal, spectral variation of the *Sphagnum papillosum*-dominated plot extracted from UAV data. This class was selected as it exhibited the highest species diversity. The boxes show the interquartile range containing the middle 50% of the data with the line representing the median and the whiskers the data range with outliers indicated as individual points. Common wavelengths for chlorophyll *a*, chlorophyll *b*, and the water index are highlighted.

Table 3
The classification results obtained using the Spectral Angle Mapper (SAM) with overall accuracies in percentage for Ilajansuo mire. Division shows mosses and mosses with mixed vegetation subdivided into models, each fed with different libraries.

SAM	Spectral Library	
	Moss	**Overall accuracy**
Model 1	Species	48 %
Model 2	Plot level	58 %
Model 3	UAV plot-level	57 %
Model 4	Species + Plot level + UAV plot-level	62 %
	Moss + mixed vegetation	
Model 5	Species	43 %
Model 6	Plot level	50 %
Model 7	UAV plot-level	48 %
Model 8	Species + Plot level + UAV plot-level	55 %

into *Sphagnum fuscum* and *Sphagnum medium* coll.

Yet, the classification using only the UAV-spectral library increased the accuracy of *Sphagnum medium* coll. by 20 %. While *Sphagnum balticum* reached a higher accuracy compared to other species with 59 %, Viitasuo mire had generally much lower overall accuracies for all runs. The hyperspectral image extent of Viitasuo mire did not cover the wet flark area, which is why some species were expected to be classified as minorities or not at all given that all spectral libraries entries from Ilajansuo site were used as a test. Excluded correctly from the accuracy assessment were the wettest classes *Sphagnum jensenii* and floating mosses as well as *Sphagnum rubellum*, which do not occur in this classified extent and in the ground truth data.

4.3. Performance along the hydrological gradient

We examined the best moss classification outcomes by setting these in relation to the moisture conditions and spectral angle used in the SAM algorithm. In Viitasuo, this means that the non-existent classes *Sphagnum jensenii* and *Sphagnum rubellum* were excluded. For both mires, we also excluded the class floating mosses from the following assessment, as these represented the wettest area with a distinct high WI and a composition of several moss species. Variables tested were the measured WTD, WI, spectral angle, species category (ground truth), and the correctness of the classification. In the following, we present the most relevant results; more details can be found in the appendix.

The correlation for Ilajansuo mire showed a significant relationship between the WI and the WTD measurements with varying degrees of significance among the classes; the *Sphagnum papillosum*-dominated class was the exception with no significant result. The strongest relationship was evident for the classes *Sphagnum balticum*, *Sphagnum jensenii*, and *Sphagnum rubellum*. Conversely, the relationship between WI and spectral angle was significant for the classes *Sphagnum fuscum, Sphagnum medium* coll., *Sphagnum majus*, and *Sphagnum papillosum*. For Viitasuo mire, the relationship between WI and WTD was highly significant for *Sphagnum balticum*, *Sphagnum. fuscum*, and *Sphagnum majus*. The highly significant relationship between WI and spectral angle was here indicated for all *Sphagnum*-dominated classes except *Sphagnum medium* coll. The Kruskal-Wallis test showed significant differences in the distribution of WI across the different moss species. The Dunn's post hoc test for pairwise comparison between the moss classes for Ilajansuo revealed significant differences in WI between *Sphagnum* mosses (*Sphagnum balticum*, *Sphagnum fuscum*, *Sphagnum medium* coll., *Sphagnum majus*, and *Sphagnum papillosum*), indicating their different preferences along the WTD gradient (Fig. 8).

Based on the Dunn's test results, *Sphagnum jensenii* and *Sphagnum rubellum* were more similar to the broader dataset and might not have carried as much ecological significance in terms of WI variation. The multi-class comparison revealed significant spectral angle differences among *Sphagnum fuscum*, *Sphagnum majus*, and *Sphagnum papillosum*. In the case of Viitasuo, significant differences in WI were found between all classes in pair-wise comparisons, this was also the case for the spectral angle among the classes. Lastly, we compared if the spectral angle and WI separately affect the classification performance for the moss-classes (i.e., correctly and incorrectly classified) using Wilcoxon rank-sum test (Mann-Whitney *U* test). The outcomes pointed out that classification performance was weaker with lower WI (Fig. 9), which means that performance was better in wetter areas for all classes except *Sphagnum balticum* and *Sphagnum papillosum* at Ilajansuo mire. Thus, it suggested that the performance of the classification is affected by the WI or spectral angle for individual classes. Due to the insufficient ground truth amount at the Viitasuo mire, this test only highlighted a statistical significance for the *Sphagnum fuscum*-dominated class. *Sphagnum majus* was excluded from this analysis in the first place, as it included only incorrectly classified values.

The logistic regression model for this research site revealed a combined impact of angle and WI for *Sphagnum jensenii*, *Sphagnum medium*

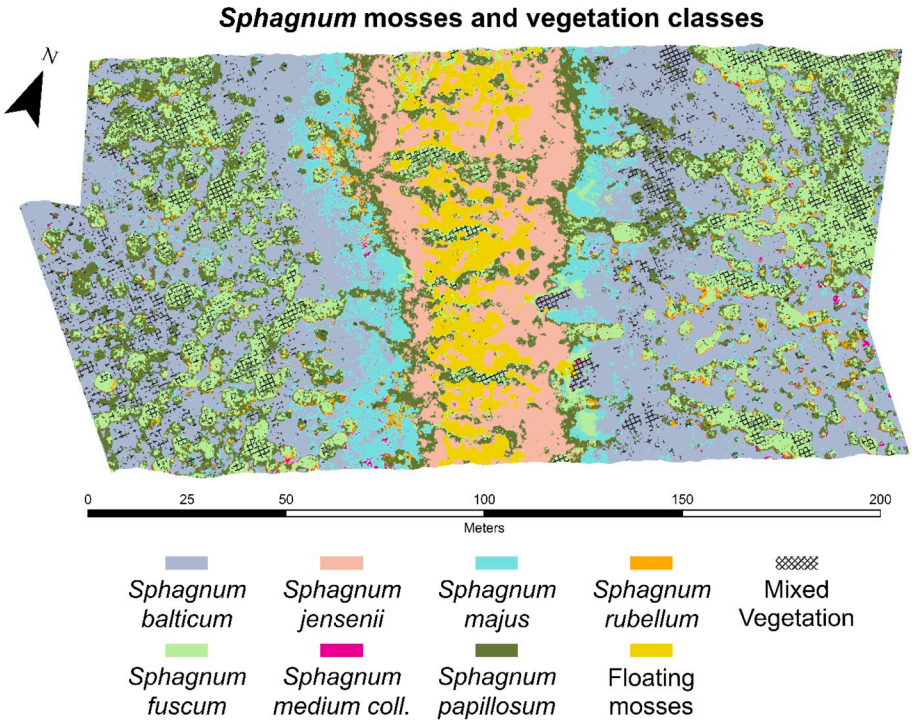

Fig. 7. Spectral Angle Mapper classification outcome of Ilajansuo mire using all spectral libraries excluding mixed vegetation. Hatched areas symbolize the proportion of mixed vegetation produced separately.

Table 4
The confusion matrix for the best moss classification result of Model 4 with the combined spectral libraries of species-, plot-, and UAV plot-level excluding the mixed vegetation entry. Entries show the number of instances used in the classification; the accuracies are in percentage.

Species	*Sph. balticum*	*Sph. fuscum*	*Sph. jensenii*	*Sph. med.* coll.	*Sph. majus*	*Sph. papillosum*	*Sph. rubellum*	Floating moss	User's Accuracy
Sph. balticum	183	0	0	14	25	12	4	0	77
Sph. fuscum	4	65	7	7	1	6	0	0	72
Sph. jensenii	10	0	91	0	30	52	0	36	42
***Sph. med.* coll.**	0	1	0	20	0	0	11	0	63
Sph. majus	28	2	16	4	70	19	9	0	47
Sph. papillosum	4	15	0	12	6	90	1	0	70
Sph. rubellum	7	32	0	14	3	0	22	0	28
Floating moss	0	0	0	0	0	0	0	96	100
Producer's Accuracy	78	57	80	28	52	50	47	73	**0.62**

coll., and *Sphagnum majus*.

5. Discussion

We explored the application of state-of-the-art hyperspectral imaging devices to establish spectral libraries of *Sphagnum* mosses for image classification purposes. In this context, we sought better understanding in the spectral complexity among and between species and the impact of hydrological circumstances in aapa mires.

5.1. Multi-source and multi-scale libraries

Our study showed that the individual spectral signatures obtained by hyperspectral imaging matched with those presented in several previous studies (Lees et al., 2020; Salko et al., 2023; Tucker et al., 2022; Ustin et al., 2009). The spectral structures were generally complex and similarly shaped with the best separation of species in the visible region of the spectra. The spectral variation that increased in random appearance particularly in the near-infrared wavelengths range marked the atmospheric interference recorded with the sensors. While the derivatives potentially pinpointed water absorption features between 940 – 960 nm (e.g. for *Sphagnum papillosum*), it must be noted that these were in the range with lowest signal-to-noise ration. Despite the spectral similarity as shown by the derivatives of *Sphagnum balticum* and *Sphagnum majus* in the visible spectral range, the misclassification among these species remained rather minimal. Regardless, at plot level both sensors showed similar spectral properties with random variation in the near-infrared range. The general and gradual spectral deviation was also here likely affected by atmospheric interference (Pillay et al., 2020). As the UAV information at plot level showed random variation across the entire spectrum, it is likely that the acquisition altitude with the variation in incoming signal has caused this. Although these spectral deviations might be small, it can still have implications for up- and downscaling in remote sensing applications. Spectrometric parameters derived from multi-source and multi-scale libraries revealed rather consistent widths and depths of absorption and reflectance features across sensors with some exceptions. This result coupled with the noise in the near-infrared wavelengths question the effectiveness of more complex classifiers (i.e., random forest) and spectral unmixing algorithms, which are commonly used for hyperspectral analysis and rely on leveraging distinct features.

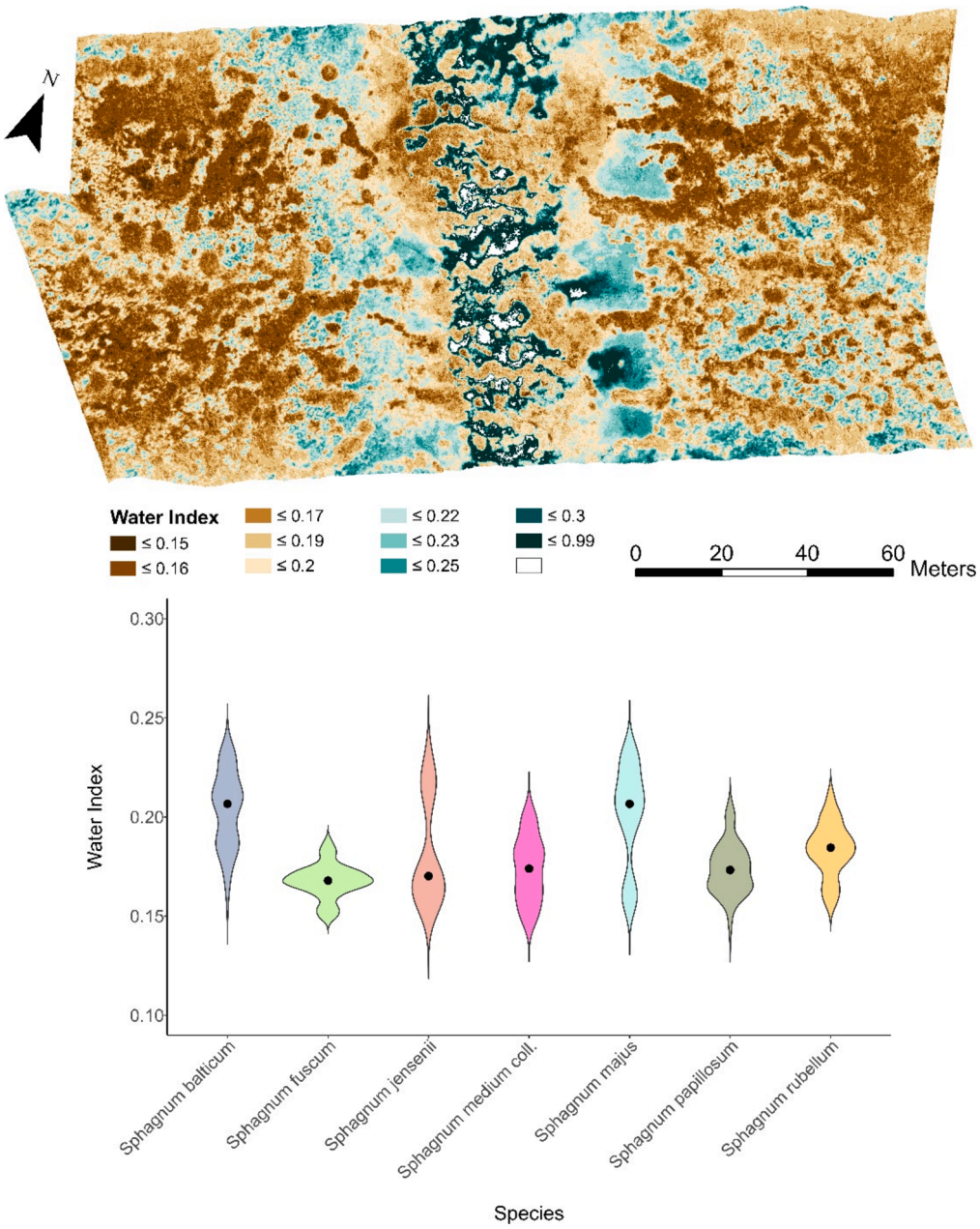

Fig. 8. The spatial variation of the water index (WI) across Ilajansuo mire (upper panel) and the moss species' location along this index as derived from the ground truth location (lower panel), with the point in the violins indicating the median value.

5.2. Spatial distribution of Sphagnum mosses

Despite the subtle differences at plot level, the results hinted that the additional spectral information gained from different altitudes and sensors may enhanced the classification results. It consequently suggests that the spectral angle threshold selection was better defined. However, the spectral angle of the true locations of *Sphagnum majus* and *papillosum* were so close that this class relation was noticeable in the accuracy assessment. Adjusting the spectral angle would have, in turn, excluded some pixels from their correct class. Generally, the accuracy can be categorized into the same reports from mire vegetation mapping (Räsänen et al., 2019; Wolff et al., 2023).

The water index was significantly higher for Viitasuo mire throughout the study extent compared to the Ilajansuo mire. We expected a moisture-induced bias in spectral response due to drier circumstances at the time of handheld hyperspectral imaging in Ilajansuo when applying this data to classify Viitasuo. Despite the low accuracy for this site, floating mosses and *Sphagnum jensenii* were correctly excluded, which is therefore a success. Further, *Sphagnum rubellum* had a low abundance as correctly shown by the classifications for both mires. Therefore, the modelling results accurately mirrored the logical arrangement of species in Ilajansuo and Viitasuo mire, although other, unsampled species occur in both sites.

During the vegetation survey, most plots exhibited 100 % moss cover, but some had less coverage or had an overstory of vascular vegetation, which is why the sampling schema and target classification can be one uncertainty cause. In situations where mixed vegetation was scattered across the plot, a mixed spectral response for the concerned pixels compared to the neighbouring moss pixels was expected, but still within an acceptable spectral threshold for the SAM algorithm. Indeed, this assumption has been confirmed, as the *Sphagnum fuscum*-dominated class with scattered vascular plant presence was sill classified

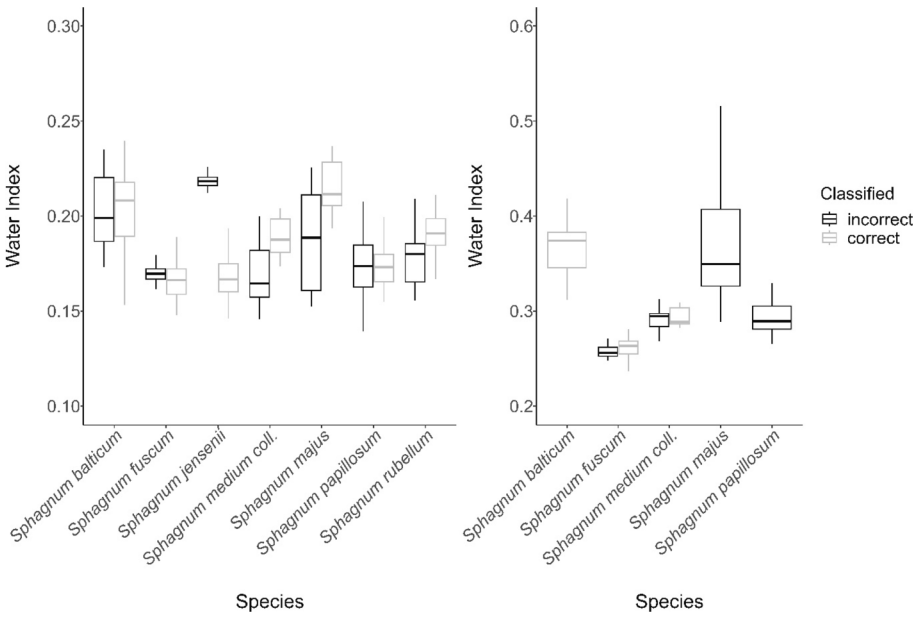

Fig. 9. The impact of the water index on the classification performance as represented by the information classified "correctly" (grey box) or "incorrectly" (black box) for the respective *Sphagnum* mosses in Ilajansuo mire (left panel) and Viitasuo mire (right panel).

accurately. Considering that SAM classified those pixels with overstory to the correct, dominant moss species successfully highlights the robustness of this simple algorithm. Upon closer inspection it became apparent that only *Sphagnum medium* coll. had some edge pixels with a high graminoid abundance that led to misclassifications, potentially affected by neighbouring litter contributing to the reflectance (Middleton et al., 2012). Although no wind persisted on the day of image acquisition, any small-scale movement of taller graminoids (alive or as litter) could have caused the plant blades outside the plot edge to lean into the plot while being recorded with the UAV. This would result in a different spectral composition than captured in the field. In this case, the sub-pixel effect likely has caused different species to be present within one pixel. On the other hand, the hyperspectral UAV resolution was 8 cm, which could have caused a mixed pixel effect for those instances with high site-heterogeneity due to the small size and intricate distribution of peatland vegetation. Although being associated with atmospheric scattering, the adjacency effect must be considered as well, as the spectral reflection of (graminoid) litter is high in magnitude and ultimately creates a strong contrast between these regions and the living *Sphagnum*-dominated vegetation adjacent to it. This issue could be mitigated by applying advanced atmospheric correction methods, such as ACTOR or FLAASH (Cooley et al., 2002; Marcello et al., 2016; Richter, 1996; Richter & Schläpfer, 2015). We recommend adjusting the sampling scheme based on the spatial resolution of the reference imagery, especially when targeting species-level classification, such as single-point recordings of the target species situated in a homogeneous area of 15 cm diameter.

5.3. Performance along the hydrological gradient

Our study suggests a species preference along a partly overlapping hydrological gradient and the possibility that hydrological circumstances may affect the separation of species. This is mirrored by our image classification performance tending to be better with increasing WI. For these aapa mires, ongoing fen-bog transitions have been discovered (Kolari and Tahvanainen, 2023). Changes in hydrological and climatic conditions may result in adjusted productivity and growth forms (i.e., longer shoots or compactness) (Bengtsson et al., 2021; Heck et al., 2021), potentially affecting also spectral properties (Clymo, 1970; Rastogi et al., 2020). Further, slowly changing microhabitat formations and shading (e.g. by vascular plants) can affect the pigmentation and ultimately the presence of *Sphagnum* species (Bonnett et al., 2010). Thus, adjustments of the angle threshold for classification are necessary in response to shifts in environmental conditions. Notably, this holds true as well for the phenological cycle and seasonal variations with changes in pigments. The "perfect" time window for vegetation modelling has been previously discussed (Cole et al., 2014b; Pang et al., 2022). Our study suggests selecting a time for image acquisition avoiding drought, excessively hot days, or an extended period of temperatures higher than average. If libraries should be used across space and time the adaption can be done in two ways. First, by collecting more (spectral) ground truth data at different time points to compensate for the wetness and moisture variation, including also short-wave infrared wavelengths to enhance species separation (Pang et al., 2020). Second, to correct for spectral variation by having several UAV- or satellite imageries. These comprehensive libraries would allow for the application across mires globally, to correct for seasonal affects, and to even model scenarios in vegetation distribution. For a more comprehensive examination of the mosses' spectral response to important drivers in mires, a similar study could be conducted in paludiculture or restoration sites.

6. Conclusions

This study presented a novel hyperspectral imaging approach to investigate spectral characteristics of *Sphagnum* mosses with multi-source, multi-scale spectral libraries (i.e., plot- and species level) and the implications for UAV-based image classification. The research examined the impact of hydrological conditions on spectral properties and on classification performance. The results highlighted the visible range of the electromagnetic spectrum as the most reliable for species separation, due to lower signal-to-noise ratio in the near-infrared wavelengths. However, the hyperspectral sensors provide narrow-band information, which benefited the classification, as the accuracies increased with higher spectral detail by fusing spectral information from species- and plot-level. Red moss species achieved the lowest classification accuracies, probably due to neighbouring graminoids and litter introducing sub-pixel and mixed-pixel effects. Most of the moss species exhibited specific hydrological gradients, revealing a significant relationship between spectral properties and water index. Interestingly, the classification performance improved for most of the species with higher

water index. The study highlights the potential of using spectral libraries for modelling. Nevertheless, it underscores the necessity to effectively integrate hydrological factors as a function of spectral signatures to compensate for variation caused by time and site conditions.

CRediT authorship contribution statement

Franziska Wolff: Writing – original draft, Visualization, Validation, Methodology, Investigation, Funding acquisition, Formal analysis, Data curation, Conceptualization. **Sandra Lorenz:** Writing – review & editing, Software, Methodology, Data curation, Conceptualization. **Pasi Korpelainen:** Writing – review & editing, Investigation, Data curation. **Anette Eltner:** Writing – review & editing, Software. **Timo Kumpula:** Writing – review & editing, Conceptualization.

Declaration of competing interest

The authors declare that they have no known competing financial interests or personal relationships that could have appeared to influence the work reported in this paper.

Data availability

Data will be made available on request.

Acknowledgments

We thank Tiina Kolari, Teemu Tahvanainen, Ville Vesakoski, and Patrik Hämäläinen for their assistance in the field. We further would like to highlight Tiina Kolari's valuable opinion on plant ecology and the experiences of Sarita Keski-Saari and Petri Nygrén in spectroscopy. This study was funded by the KONE foundation in the context of the PhD project of F. Wolff. This work received financial support from the UEF Water research program, which is jointly funded by the Saastamoinen Foundation, the Wihuri Foundation, and the Olvi Foundation.

Appendix A. Supplementary material

Supplementary data to this article can be found online at https://doi.org/10.1016/j.jag.2024.104201.

References

Andrus, R.E., 1986. Some aspects of Sphagnum ecology. Can. J. Bot. 64 (2), 416–426. https://doi.org/10.1139/b86-057.

Andrus, R.E., Wagner, D.J., Titus, J.E., 1983. Vertical zonation of Sphagnum mosses along hummock-hollow gradients. Can. J. Bot. 61 (12), 3128–3139. https://doi.org/10.1139/b83-352.

Arkimaa, H., Middleton, M., Hyvönen, E., Kuosmanen, V., Laitinen, J., Sutinen, R., 2005. Mire site type mapping of boreal peatlands with hyperspectral airborne Hymap in Northern Finland. EARSeL and Warsaw University, Warsaw 2005. Proceedings of 4th EARSeL Workshop on Imaging Spectroscopy. New quality in environmental studies.

Arkimaa, H., Laitinen, J., Korhonen, R., Moisanen, M., Hirvasniemi, T., Kuosmanen, V., 2009. Spectral reflectance properties of Sphagnum moss species in Finnish mires.

Bengtsson, F., Rydin, H., Baltzer, J.L., Bragazza, L., Bu, Z.-J., Caporn, S.J.M., Dorrepaal, E., Flatberg, K.I., Galanina, O., Gałka, M., Ganeva, A., Goia, I., Goncharova, N., Hájek, M., Haraguchi, A., Harris, L.I., Humphreys, E., Jirošek, M., Kajukało, K., Karofeld, E., Koronatova, N.G., Kosykh, N.P., Laine, A.M., Lamentowicz, M., Lapshina, E., Limpens, J., Linkosalmi, M., Ma, J.-Z., Mauritz, M., Mitchell, E.A.D., Munir, T.M., Natali, S.M., Natcheva, R., Payne, R.J., Philippov, D. A., Rice, S.K., Robinson, S., Robroek, B.J.M., Rochefort, L., Singer, D., Stenøien, H.K., Tuittila, E.-S., Vellak, K., Waddington, J.M., Granath, G., 2021. Environmental drivers of *Sphagnum* growth in peatlands across the Holarctic region. J. Ecol. 109, 417–431. https://doi.org/10.1111/1365-2745.13499.

Berland, H., Andersen, Ø.M., 2021. Characterization of a natural, stable, reversible and colourful anthocyanidin network from sphagnum moss based mainly on the yellow trans-chalcone and red flavylium cation forms. Molecules 2, 3. https://doi.org/10.3390/molecules26030709.

Bonnett, S.A.F., Ostle, N., Freeman, C., 2010. Short-term effect of deep shade and enhanced nitrogen supply on Sphagnum capillifolium morphophysiology. Plant Ecol. 207, 347–358. https://doi.org/10.1007/s11258-009-9678-0.

Breeuwer, A., Heijmans, M.M.P.D., Robroek, B.J.M., Berendse, F., 2008. The effect of temperature on growth and competition between Sphagnum species. Oecologia 156, 155–167. https://doi.org/10.1007/s00442-008-0963-8.

Bryant, R.G., Baird, A.J., 2003. The spectral behaviour of Sphagnum canopies under varying hydrological conditions. Geophys. Res. Lett. 30, 1134. https://doi.org/10.1029/2002GL016053.

Bubier, J.L., Rock, B.N., Crill, P.M., 1997. Spectral reflectance measurements of boreal wetland and forest mosses. J. Geophys. Res. 102, 29483–29494. https://doi.org/10.1029/97JD02316.

Caturegli, L., Matteoli, S., Gaetani, M., Grossi, N., Magni, S., Minelli, A., Corsini, G., Remorini, D., Volterrani, M., 2020. Effects of water stress on spectral reflectance of bermudagrass. Sci. Rep. 10, 15055. https://doi.org/10.1038/s41598-020-72006-6.

Chen, M., Blankenship, R. E., 2011. Expanding the solar spectrum used by photosynthesis, Trends Plant Sci. 16, 427-431. DOI: 10.1016/j.tplants.2011.03.011.

Clevers, J.G.P.W., Kooistra, L., Schaepman, M.E., 2008. Using spectral information from the NIR water absorption features for the retrieval of canopy water content. Int. J. Appl. Earth Obs. Geoinf. 10, 388–397. https://doi.org/10.1016/j.jag.2008.03.003.

Clymo, R.S., 1970. The Growth of Sphagnum: Methods of Measurement. J. Ecol. 58, 13–49. JSTOR, DOI: 10.2307/2258168.

Cole, B., McMorrow, J., Evans, M., 2014a. Empirical Modelling of Vegetation Abundance from Airborne Hyperspectral Data for Upland Peatland Restoration Monitoring. Remote Sens. 6, 716–739. https://doi.org/10.3390/rs6010716.

Cole, B., McMorrow, J., Evans, M., 2014b. Spectral monitoring of moorland plant phenology to identify a temporal window for hyperspectral remote sensing of peatland. ISPRS J. Photogramm. Remote Sens. 90, 49–58. https://doi.org/10.1016/j.isprsjprs.2014.01.010.

Cooley, T., Anderson, G.P., Felde, G.W., Hoke, M.L., Ratkowski, A.J., Chetwynd, J.H., Gardner, J.A., Adler-Golden, S.M., Matthew, M.W., Berk, A., Bernstein, L.S., Acharya, P.K., Miller, D., Lewis, P., 2002. FLAASH, a MODTRAN4-based Atmospheric Correction Algorithm. Its Application and Validation. Proceedings of the IEEE International Geoscience and Remote Sensing Symposium (IGARSS).

Cristóbal, J., Graham, P., Prakash, A., Buchhorn, M., Gens, R., Guldager, N., Bertram, M., 2021. Airborne hyperspectral data acquisition and processing in the arctic: a pilot study using the hyspex imaging spectrometer for wetland mapping. Remote Sens. 13, 1178. https://doi.org/10.3390/rs13061178.

Erudel, T., Fabre, S., Houet, T., Mazier, F., Briottet, X., 2017. Criteria comparison for classifying peatland vegetation types using in situ hyperspectral measurements. Remote Sens. 9, 7. https://doi.org/10.3390/rs9070748.

Granath, G., Strengbom, J., Rydin, H., 2010. Rapid ecosystem shifts in peatlands: linking plant physiology and succession. Ecology 91, 3047–3056. https://doi.org/10.1890/09-2267.1.

Granlund, L., Keski-Saari, S., Kumpula, T., Oksanen, E., Keinänen, M., 2018. Imaging lichen water content with visible to mid-wave infrared (400–5500 nm) spectroscopy. Remote Sens. Environ. 216, 301–310. https://doi.org/10.1016/j.rse.2018.06.041.

Granlund, L., Vesakoski, V., Sallinen, A., Kolari, T.H.M., Wolff, F., Tahvanainen, T., 2022. Recent Lateral Expansion of *Sphagnum* Bogs Over Central Fen Areas of Boreal Aapa Mire Complexes. Ecosystems 25, 1455–1475. https://doi.org/10.1007/s10021-021-00726-5.

Hájek, T., Ballance, S., Limpens, J., Zijlstra, M., Verhoeven, J.T.A., 2011. Cell-wall polysaccharides play an important role in decay resistance of Sphagnum and actively depressed decomposition in vitro. Biogeochemistry 103, 45–57. https://doi.org/10.1007/s10533-010-9444-3.

Harris, A., 2008. Spectral reflectance and photosynthetic properties of Sphagnum mosses exposed to progressive drought. Ecohydrology 1 (1), 35–42. https://doi.org/10.1002/eco.5.

Harris, A., Bryant, R.G., Baird, A.J., 2005. Detecting near-surface moisture stress in *Sphagnum* spp. Remote Sens. Environ. 97, 371–381. https://doi.org/10.1016/j.rse.2005.05.001.

Harris, A., Charnock, R., Lucas, R.M., 2015. Hyperspectral remote sensing of peatland floristic gradients. Remote Sens. Environ. 162, 99–111. https://doi.org/10.1016/j.rse.2015.01.029.

Heck, M.A., Melková, I., Posten, C., Decker, E.L., Reski, R., 2021. Medium optimization for biomass production of three peat moss (Sphagnum L.) species using fractional factorial design and response surface methodology. Bioresour. Technol. Rep. 15, 100729. https://doi.org/10.1016/j.biteb.2021.100729.

Hughes, G., 1968. On the mean accuracy of statistical pattern recognizers. IEEE Trans. Inf. Theory 14, 55–63. https://doi.org/10.1109/tit.1968.1054102.

Johnson, M.G., Granath, G., Tahvanainen, T., Pouliot, R., Stenøien, H.K., Rochefort, L., Rydin, H., Shaw, A.J., 2015. Evolution of niche preference in Sphagnum peat mosses. Evol. 69, 90–103. https://doi.org/10.1111/evo.12547.

Kaufman, Y.J., 1984. Atmospheric effect on spatial resolution of surface imagery: errata. Appl. Opt. 23, 4164–4172. https://doi.org/10.1364/AO.23.004164.

Kokkonen, N., Laine, A.M., Männistö, E., Korrensalo, A., Tuittila, E.-S., 2022. Two Mechanisms Drive Changes in Boreal Peatland Photosynthesis Following Long-Term Water Level Drawdown: Species Turnover and Altered Photosynthetic Capacity. Ecosystems 25, 1601–1618. https://doi.org/10.1007/s10021-021-00736-3.

Kolari, T.H.M., Tahvanainen, T., 2023. Inference of future bog succession trajectory from spatial chronosequence of changing aapa mires. Ecol. Evol. 13, e09988.

Kolari, T.H.M., Korpelainen, P., Kumpula, T., Tahvanainen, T., 2021. Accelerated vegetation succession but no hydrological change in a boreal fen during 20 years of recent climate change. Ecol. Evol. 11, 7602–7621. https://doi.org/10.1002/ece3.7592.

Kolari, T.H.M., Sallinen, A., Wolff, F., Kumpula, T., Tolonen, K., Tahvanainen, T., 2022. Ongoing Fen-Bog Transition in a Boreal Aapa Mire Inferred from Repeated Field Sampling, Aerial Images, and Landsat Data. Ecosystems 25, 1166–1188. https://doi.org/10.1007/s10021-021-00708-7.

Korrensalo, A., Hájek, T., Vesala, T., Mehtätalo, L., Tuittila, E.-S., 2016. Variation in photosynthetic properties among bog plants. Botany 94, 1127–1139. https://doi.org/10.1139/cjb-2016-0117.

Kruse, F.A., Lefkoff, A.B., Boardman, J.W., Heidebrecht, K.B., Shapiro, A.T., Barloon, P. J., Goetz, A.F.H., 1993. The spectral image processing system (SIPS)—interactive visualization and analysis of imaging spectrometer data. Remote Sens. Environ. 44, 145–163. https://doi.org/10.1016/0034-4257(93)90013-n.

Laine, A.M., Juurola, E., Hájek, T., Tuittila, E.-S., 2011. Sphagnum growth and ecophysiology during mire succession. Oecologia 167, 1115–1125. https://doi.org/10.1007/s00442-011-2039-4.

Lees, K.J., Artz, R.R.E., Khomik, M., Clark, J.M., Ritson, J., Hancock, M.H., Cowie, N.R., Quaife, T., 2020. Using Spectral Indices to Estimate Water Content and GPP in *Sphagnum* Moss and Other Peatland Vegetation. IEEE Trans Geosci. Remote Sens. 58, 4547–4557. https://doi.org/10.1109/TGRS.2019.2961479.

Lichtenthaler, H.K., Buschmann, C., 2001. Chlorophylls and Carotenoids: Measurement and Characterization by UV-VIS Spectroscopy. Curr. Protoc. Food Anal. Chem. 1, F4.3.1–F4.3.8. https://doi.org/10.1002/0471142913.faf0403s01.

Marcello, J., Eugenio, F., Perdomo, U., Medina, A., 2016. Assessment of Atmospheric Algorithms to Retrieve Vegetation in Natural Protected Areas Using Multispectral High Resolution Imagery. Sensors 16, 1624. https://doi.org/10.3390/s16101624.

Mathijssen, P.J.H., Gałka, M., Borken, W., Knorr, K.-H., 2019. Plant communities control long term carbon accumulation and biogeochemical gradients in a Patagonian bog. Sci. Total Environ. 684, 670–681. https://doi.org/10.1016/j.scitotenv.2019.05.310.

Meingast, K.M., Falkowski, M.J., Kane, E.S., Potvin, L.R., Benscoter, B.W., Smith, A.M.S., Bourgeau-Chavez, L.L., Miller, M.E., 2014. Spectral detection of near-surface moisture content and water-table position in northern peatland ecosystems. Remote Sens. Environ. 152, 536–546. https://doi.org/10.1016/j.rse.2014.07.014.

Middleton, M., Närhi, P., Arkimaa, H., Hyvönen, E., Kuosmanen, V., Treitz, P., Sutinen, R., 2012. Ordination and hyperspectral remote sensing approach to classify peatland biotopes along soil moisture and fertility gradients. Remote Sens. Environ. 124, 596–609. https://doi.org/10.1016/j.rse.2012.06.010.

Neta, T., Cheng, Q., Bello, R.L., Hu, B., 2011. Development of new spectral reflectance indices for the detection of lichens and mosses moisture content in the Hudson Bay Lowlands Canada. Hydrol. Process. 25, 933–944. https://doi.org/10.1002/hyp.7878.

Pang, Y., Huang, Y., Zhou, Y., Xu, J., Wu, Y., 2020. Identifying spectral features of characteristics of *Sphagnum* to assess the remote sensing potential of peatlands: A case study in China. Mires Peat 26, 25. https://doi.org/10.19189/MaP.2019.OMB.StA.1834.

Pang, Y., Räsänen, A., Lindholm, V., Aurela, M., Virtanen, T., 2022. Detecting peatland vegetation patterns with multi-temporal field spectroscopy. Gisci. Remote Sens. 59, 2111–2126. https://doi.org/10.1080/15481603.2022.2152303.

Penuelas, J., Pinol, J., Ogaya, R., Filella, I., 1997. Estimation of plant water concentration by the reflectance Water Index WI (R900/R970). Int. J. Remote Sens. 18, 2869–2875. https://doi.org/10.1080/014311697217396.

Pillay, R., Picollo, M., Hardeberg, J.Y., George, S., 2020. Evaluation of the data quality from a round-robin test of hyperspectral imaging systems. Sensors 20, 3812. https://doi.org/10.3390/s20143812.

R Core Team (2022). R: A language and environment for statistical computing (Version 4.2.3) [Software]. R Foundation for Statistical Computing. https://www.R-project.org/.

Räsänen, A., Juutinen, S., Tuittila, E.-S., Aurela, M., Virtanen, T., 2019. Comparing ultra-high spatial resolution remote-sensing methods in mapping peatland vegetation. J. Veg. Sci. 30, 1016–1026. https://doi.org/10.1111/jvs.12769.

Räsänen, A., Aurela, M., Juutinen, S., Kumpula, T., Lohila, A., Penttilä, T., Virtanen, T., 2020. Detecting northern peatland vegetation patterns at ultra-high spatial resolution. Remote Sens. Ecol. 6, 457–471. https://doi.org/10.1002/rse2.140.

Rastogi, A., Antala, M., Gąbka, M., Rosadziński, S., Stróżecki, M., Brestic, M., Juszczak, R., 2020. Impact of warming and reduced precipitation on morphology and chlorophyll concentration in peat mosses (Sphagnum angustifolium and S. fallax). Sci. Rep. 10, 8592. https://doi.org/10.1038/s41598-020-65032-x.

Rautiainen, M., Lukeš, P., Homolová, L., Hovi, A., Pisek, J., Mõttus, M., 2018. Spectral Properties of Coniferous Forests: A Review of In Situ and Laboratory Measurements. Remote Sens. 10, 207. https://doi.org/10.3390/rs10020207.

Richter, R.A., 1996. A spatially adaptive fast atmospheric correction algorithm. Int. J. Remote Sens. 17, 1201–1214.

Richter, R., Schläpfer, D., 2015. Atmospheric/Topographic Correction for Satellite Imagery: ATCOR-2/3 User Guide; DLR Report. Wil, Switzerland, ReSe Applications Schläpfer.

Robroek, B.J., Limpens, J., Breeuwer, A., Schouten, M.G.C., 2007. Effects of water level and temperature on performance of four Sphagnum mosses. Plant Ecol. 190, 97–107. https://doi.org/10.1007/s11258-006-9193-5.

Salko, S.-S., Juola, J., Burdun, I., Vasander, H., Rautiainen, M., 2023. Intra- and interspecific variation in spectral properties of dominant *Sphagnum* moss species in boreal peatlands. Ecol. Evol. 13, e10197.

Schaepman-Strub, G., Limpens, J., Menken, M., Bartholomeus, H.M., Schaepman, M.E., 2009. Towards spatial assessment of carbon sequestration in peatlands: spectroscopy based estimation of fractional cover of three plant functional types. Biogeosciences 6, 275–284. https://doi.org/10.5194/bg-6-275-2009.

Schmidt, K.S., Skidmore, A.K., 2003. Spectral discrimination of vegetation types in a coastal wetland. Remote Sens Environ. 85, 92–108. https://doi.org/10.1016/S0034-4257(02)00196-7.

Exelis Visual Information Solutions, 2022. ENVI version 5.6.3. Boulder, Colorado: Exelis Visual Information Solutions.

Stuart, M.B., Davies, M., Hobbs, M.J., McGonigle, A.J.S., Willmott, J.R., 2022. Peatland Plant Spectral Response as a Proxy for Peat Health, Analysis Using Low-Cost Hyperspectral Imaging Techniques. Remote Sens. 14, 16. https://doi.org/10.3390/rs14163846.

Tahvanainen, T., Tolonen, K., 2004. Patterns of species responses to the water-table depth gradient in Finnish mires. Conference: Wise use of peatlands, 12th International Peat Congress, Tampere, Finland. Volume: Proceedings of the 12th International Peat Congress (2) 925-930.

Thiele, S.T., Lorenz, S., Kirsch, M., Acosta, I.C.C., Tusa, L., Herrmann, E., Möckel, R., Gloaguen, R., 2021. Multi-scale, multi-sensor data integration for automated 3-D geological mapping. Ore Geol. Rev. 136, 104252. https://doi.org/10.1016/j.oregeorev.2021.104252.

Tucker, C., O'Neill, A., Meingast, K., Bourgeau-Chavez, L., Lilleskov, E., Kane, E.S., 2022. Spectral indices of vegetation condition and soil water content reflect controls on CH_4 and CO_2 exchange in *Sphagnum*-dominated northern peatlands. e2021JG006486 J. Geophys. Res. Biogeosci. 127. https://doi.org/10.1029/2021JG006486.

Ustin, S.L., Gitelson, A.A., Jacquemoud, S., Schaepman, M., Asner, G.P., Gamon, J.A., Zarco-Tejada, P., 2009. Retrieval of foliar information about plant pigment systems from high resolution spectroscopy. Remote Sens. of Environ. 113 (Suppl. 1), S67–S77.

Väliranta, M., Salojärvi, N., Vuorsalo, A., Juutinen, S., Korhola, A., Luoto, M., Tuittila, E.-S., 2017. Holocene fen–bog transitions, current status in Finland and future perspectives. Holocene 27, 752–764. https://doi.org/10.1177/0959683616670471.

Ward, S.E., Orwin, K.H., Ostle, N.J., Briones, M.J.I., Thomson, B.C., Griffiths, R.I., Oakley, S., Quirk, H., Bardgett, R.D., 2015. Vegetation exerts a greater control on litter decomposition than climate warming in peatlands. Ecology 96, 113–123. https://doi.org/10.1890/14-0292.1.

Wolff, W., Kolari, T.H.M., Villoslada, M., Tahvanainen, T., Korpelainen, P., Zamboni, P. A.P., Kumpula, T., 2023. RGB vs. Multispectral imagery: Mapping aapa mire plant communities with UAVs. Ecol. Indic. 148, 110140. https://doi.org/10.1016/j.ecolind.2023.110140.